Synthesis-controlled polymorphism, magnetic and electrochemical properties of $Li_3Co_2SbO_6$

Alex J Brown,[1] Qingbo Xia,[1] Maxim Avdeev,[1,2] Brendan J Kennedy[1] and Chris D Ling[1,*]

[1] *School of Chemistry, The University of Sydney, Sydney 2006, Australia*

[2] *Australian Centre for Neutron Science, Australian Nuclear Science and Technology Organisation, Kirrawee 2232, Australia*

Abstract

$Li_3Co_2SbO_6$ is found to adopt two highly distinct structural forms: a pseudohexagonal (monoclinic *C*2/*m*) layered O3-$LiCoO_2$ type phase with "honeycomb" 2:1 ordering of Co and Sb; and an orthorhombic *Fddd* phase, isostructural with $Li_3Co_2TaO_6$ but with the addition of significant Li/Co ordering. Pure samples of both phases can be obtained by conventional solid-state synthesis via a precursor route using Li_3SbO_4 and CoO, by controlling particle size, initial lithium excess, and reaction time. Both phases show relatively poor performance as lithium-ion battery cathode materials in their as-made states, but complex and interesting low-temperature magnetic properties. The honeycomb phase is the first of its type to show A-type antiferromagnetic order (ferromagnetic planes, antiferromagnetically coupled) below T_N = 14 K. Isothermal magnetisation and in-field neutron diffraction below T_N show clear evidence for a metamagnetic transition at H ~ 0.7 T to 3-D ferromagnetic order. The orthorhombic phase orders antiferromagnetically below T_N = 112 K, then undergoes two more transitions at 80 K and 60. Neutron diffraction data show that the ground state is incommensurate.

Introduction

Layered transition metal oxides of the type A_xMO_2, where A is an alkali metal and M is a transition metal, are among the most intensively studied class of solid-state compounds in recent years.[1] They are the dominant materials used as positive electrode (cathode) materials for Li-ion batteries due to their high performance combined with relative ease of synthesis, high stability and high melting points. They also display a wide variety of other fascinating physical phenomena. For example, Na_xCoO_2 shows interesting thermoelectric properties and favourable electrochemical properties for use as a positive electrode in Na-ion batteries;[2–4] and becomes superconducting ($T_c \sim 5$ K)[5] after intercalating water as $Na_{0.3}CoO_2 \bullet 1.4H_2O$.

The key structural motif of the A_xMO_2 oxides is hexagonal (or pseudo-hexagonal) layers of edge-sharing MO_6 octahedra, alternating with layers of A cations in either octahedral or trigonal coordination depending on the MO_6 layer stacking arrangement. Substituting 1/3 of the M sites with another element, M', can gives rise to ordered superstructures with the general formula $A_xM_2M'O_6$, where each $M'O_6$ octahedron is surrounded by six edge-sharing MO_6 octahedra to form "honeycomb" layers. The honeycomb arrangement is stabilised when the charge difference between M and M' is large but the size difference is relatively small: specifically, M = Mg^{2+}, Co^{2+}, Ni^{2+}, Cu^{2+}, Zn^{2+} and M'= Sb^{5+} Bi^{5+} or Te^{6+}. The first reported $A_3M_2M'O_6$ honeycomb-type phases were $Li_3Zn_2SbO_6$ and $Li_3Zn_2BiO_6$ in 1990.[6] $Li_3Zn_2SbO_6$ has Zn^{2+}/Sb^{5+} octahedral honeycomb ordering with alternating metal layers separated by Li^+ layers. Since then, the number of known examples has expanded to include most of the combinations $A_3M_2M'O_6$ (A = Na, Li; M = Mg, Co, Ni, Cu, Zn; M' = Sb, Bi), $A_2M_2TeO_6$ (A = Li, Na, K; M = Co, Cu, Mg, Zn, Ni) and Li_4MTeO_6 (M = Co, Ni, Cu, Zn).[6–23]

However, the above $A_3M_2M'O_6$ stoichiometries do not always give rise to honeycomb-ordered phases. In some cases, the honeycomb phase competes with a rock-salt type ordered arrangement commonly referred to as an orthorhombic *Fddd* superstructure, of which the first reported example is $Li_3Co_2TaO_6$.[24] Examples of the *Fddd* phase include $Li_3M_2M'O_6$ (M = Ni, Co, Mg; M' = Nb, Ta, Sb).[24–26] $Li_3Ni_2SbO_6$ has been reported in both honeycomb and orthorhombic superstructure phases;[24] however, Nalbandyan and co-workers reported that they were unable to reproduce the latter despite their comprehensive work on the structure and magnetism of the honeycomb phase of the same stoichiometry,[9] and we were also unsuccessful in preparing this using either conventional reagents or a Li_3SbO_4 precursor. More recently, $Li_3Co_{1.06}TeO_6$ was reported to crystallise in an orthorhombic *Fddd* space

group with similar unit cell dimensions to other $Li_3M_2M'O_6$ rock salt-type superstructures,[27] but with Co^{2+} and Co^{3+} mixed valence states.

More recently, K^+ honeycomb tellurates $K_2M_2TeO_6$ (M = Ni, Mg, Zn, Co and Cu) have been synthesised and studied as rechargeable K-ion battery cathode materials.[28] $K_2Ni_2TeO_6$ can reversibly insert K^+ at voltages of ~4 V and has a discharge/charge capacity of ~ 70 mAh g^{-1}. It also shows very good ionic conductivity of 0.01 mS cm^{-1} at 298 K.[28]

Another significant area of interest in the honeycomb oxides has been their low-temperature magnetic properties. Hexagonal arrangements of magnetic M cations around a non-magnetic M' cation can lead to frustrated magnetic ground states; and the relatively long and weak inter-layer magnetic interactions means that the systems are pseudo-low dimensional and highly susceptible to competing quantum fluctuations.[29] Honeycomb oxides have been reported to show spin-glass behaviour and spin-flop transitions, in addition to a long-range-ordered 'zig-zag' antiferromagnetic (AFM) ground state that breaks hexagonal symmetry[8,12,13,29] in preference to the more intuitive Néel state that would preserve it. Finally, recent theoretical work suggests that Co^{2+} d^7 honeycomb compounds could stabilise Kitaev exchange and give rise to a quantum spin-liquid state.[30]

The present work concerns $Li_3Co_2SbO_6$, which has been relatively under-represented in the literature on the $Li_3M_2SbO_6$ honeycomb-type phases. An XRD pattern deposited with the ICDD (Powder Diffraction File 00-58-637) reports a $C2/m$ unit cell (a common monoclinic distortion of the hexagonal honeycomb phases), and another (Powder Diffraction File 00-58-770) reports an *Fddd* unit cell and suggests that the structure type may be analogous to $Li_3Ni_2TaO_6$. Magnetic properties and EPR spectra for a honeycomb phase of $Li_3Co_2SbO_6$ were reported in a conference proceeding from 2013[31], but the synthetic conditions and electrochemistry were not described. However, while the present work was under review, these authors (Stratan et al.) published a full journal article[32] expanding on their results and describing the synthesis of the honeycomb phase of $Li_3Co_2SbO_6$ by ion exchange from the Na analogue, $Na_3Co_2SbO_6$. Where our results overlap, we therefore now draw comparisons to those published in the latter article.

Here, we report the solid-state synthesis (via a precursor route), crystal structure, magnetism and basic electrochemical performance of $Li_3Co_2SbO_6$ in two polymorphs: an O3-type honeycomb phase; and an *Fddd* orthorhombic phase.

Experimental

$Li_3Co_2SbO_6$ was prepared using conventional solid-state methods. Starting materials were obtained from commercial suppliers. Li_2CO_3 (99.9%, Sigma-Aldrich) was dried at 120 °C prior to reaction to avoid moisture contamination. 5 g samples of Li_3SbO_4 precursor were prepared based on methods previously described in the literature.[33,34] Li_2CO_3 and Sb_2O_3 (99%, BDH Chemicals) were mixed in the relevant stochiometric ratios and ground with acetone using an agate mortar and pestle. The ground paste was dried before being pressed into a 20 mm pellet at ~35 MPa. The pellet was then reacted at an initial temperature of 650 °C for 2 hours, before calcining at 950 °C for 12 hours. Li_3SbO_4 was obtained as a cream-coloured polycrystalline sample and characterised by X-ray diffraction (XRD). 5-6 g samples of CoO were synthesised from Co_3O_4 (99.9%, Sigma-Aldrich) by heating finely ground. Co_3O_4 as a loose powder at 1050 °C under flowing Ar in a tube furnace for 12 h. The resulting brown powder of CoO was confirmed by XRD.

2-3 g samples of the honeycomb phase of $Li_3Co_2SbO_6$ were prepared from a stochiometric 1:2 mixture of Li_3SbO_4 and CoO. The mixture was ground using an agate mortar and pestle before being pressed into a rod at ~40 MPa using a hydrostatic press. The rod was placed in an alumina boat, heated to 1100 °C under flowing Ar at a rate of 6 °C/min, held at that temperature for 90 min then furnace-cooled to room temperature. These short reaction times were found to produce the most crystalline samples and minimise evaporative loss of Li. The resulting compound was a pinkish-red powder.

2-3 g samples of the orthorhombic phase of $Li_3Co_2SbO_6$ were prepared in a similar manner. Li_3SbO_4 and CoO were mixed with Li_2CO_3 in 5% excess by ball-milling for 3 h at 400 rpm. The mixture was then pressed into a rod at ~40 MPa using a hydrostatic press. The rod was heated to 1100 °C, in an alumina boat under flowing Ar, at a rate of 8 °C/min. The temperature was held at 1100 °C for 3 h then furnace-cooled to room temperature. We note that the resulting sample was a lighter-coloured pink powder compared to the honeycomb phase; however, this may be due to changes in the morphology and/or density, rather than the electronic structure. Stratan et al.[32] described their ion-exchanged sample of the honeycomb phase as reddish-brown in colour.

Polycrystalline samples were characterised by X-ray powder diffraction (XRD) at Sydney Analytical, a core research facility at the University of Sydney. Data were collected on a PANalytical X'Pert Pro MPD, using non-monochromated Cu Kα radiation ($K\alpha_1$, λ = 1.5406

Å; $K\alpha_2$, λ = 1.5444 Å) with a Ni filter. Data were collected in Bragg-Brentano θ:2θ geometry, with a voltage of 45 kV and current of 40 mA, at a scanning rate of 0.045 2θ/s, typically over the range $5 < 2\theta < 90$ °2θ.

The orthorhombic phase of $Li_3Co_2SbO_6$ was further characterised by low-temperature XRD using a STOE Stadi P diffractometer with a Mo-$K_{\alpha 1}$ source (λ = 0.7093 Å), monochromatised by (111) Ge. The sample was mounted on an Al-coated bronze sample holder. Temperatures were achieved using an Oxford Cryosystems PheniX with data measured to 12 K, in steps of 20 K with collection times of 3 h per step. Data were collected in the range $5 < 2\theta < 55$ ° using a Dectris MYTHEN2 1K microstrip detector.

Structures were refined using the Rietveld method as implemented in TOPAS (V5). The background was fit using a 8th-order Chebychev polynomial. For the honeycomb phase, preferred orientation (PO) was modelled using the spherical harmonics function (Järvinen, 1993) found in TOPAS.[35,36] The peaks were modelled using the pseudo-Voigt TCHZ function.

Magnetic susceptibilities were measured using a Quantum Design Physical Properties Measurement System (PPMS). Temperature-dependent DC magnetic susceptibility measurements were taken under zero field-cooled (ZFC) and field-cooled (FC) conditions over the range 2-300 K, in an applied field of 0.1 T. Isothermal field-dependent magnetisation data were collected to ± 3 T at constant temperatures.

Neutron powder diffraction (NPD) measurements were carried out using the high-resolution diffractometer ECHIDNA[37] at the OPAL facility, Australian Nuclear Science and Technology Organisation (ANSTO), using neutrons of wavelength 2.4395 Å. The powder samples were sealed in vanadium cans and low-temperature data were collected at 3 K and 20 K for the honeycomb phase, and 3 K and 125 K for the orthorhombic phase. The magnetic structures were analysed by Rietveld refinement using TOPAS. For the magnetic structure refinements of the monoclinic phase, the nuclear structure model refined against 20 K NPD data was selected as the parent structure (undistorted) and symmetry representation analysis was applied using ISODISTORT[38] based on the observed magnetic supercell reflections.

Both $Li_3Co_2SbO_6$ phases were tested as Li-ion battery cathode materials. Composite electrodes were prepared by mixing with carbon black and polyvinylidene fluoride (PVDF) binder (80:10:10 wt%) and casting onto an aluminium foil current collector. Coin cells were made in an Ar-filled glovebox, with 1 M $LiPF_6$ in ethylene carbonate and diethyl carbonate

(1:1 volume ratio) used as the electrolyte. Li metal was the counter electrode, separated from the $Li_3Co_2SbO_6$ electrode by a fibre glass separator. Electrochemical performance of the coin-cells was tested with a Neware BTS 4000 battery cycler, at 25 °C, with a constant current of 0.04 mA and voltage ranging from 2 to 4.2 V.

Results and Discussion

Synthesis

Initial attempts to prepare $Li_3Co_2SbO_6$ using a solid-state method similar to that described for the Na analogue, $Na_3Co_2SbO_6$,[8] were unsuccessful. Reaction in air or under flowing O_2 at temperatures ≤1000 °C resulted in poorly crystalline honeycomb phases with very pronounced peak broadening and intensity loss due to layer-stacking faults, and an $LiCoO_2$ impurity, suggesting evaporative loss of Li and Sb. Higher reaction temperatures caused complete decomposition, with only deep blue $CoAl_2O_4$ remaining on the alumina crucible walls.

We therefore developed an alternative synthesis route where a precursor phase Li_3SbO_4 [33,34] was reacted with freshly prepared CoO. This precursor route has a number of favourable aspects. Sb is already in the 5+ oxidation state (vs. 3+ in the conventional solid-state reagent, Sb_2O_3), which allows the reaction to be performed in the absence of O_2 (in this case, under Ar). In turn, the absence of O_2 allows us to use CoO with Co in the desired 2+ oxidation state, avoiding the formation of Co_3O_4. Finally, Li_3SbO_4 has a higher melting point than either Li_2CO_3 or Sb_2O_3, which minimises the evaporative loss of Li and Sb and allows us to use higher reaction temperatures for shorter times (90 minutes). Longer annealing times at these temperatures led to decomposition, as for the direct (non-precursor) route.

The orthorhombic phase, which we first identified as an impurity in the synthesis of the honeycomb phase, was isolated after empirically testing different reaction conditions. We found two factors that favoured the formation of the orthorhombic phase: a small (5%) excess of Li_2CO_3; and ball-milling the reagents prior to pressing into rods. Significantly longer annealing times under the same conditions, or post-annealing of the orthorhombic phase, led to decomposition rather than conversion to the honeycomb phase. Taken together, these observations suggest that the orthorhombic phase is favoured when it can initially form Li-rich, but is also more susceptible to Li and Sb loss at high temperatures.

Structural refinements

The structure of each $Li_3Co_2SbO_6$ phase was analysed by Rietveld-refinement against XRD data. The honeycomb phase was indexed in the monoclinic space group *C*2/*m*, isostructural with $Na_3Co_2SbO_6$, which has an O3-type layer stacking arrangement. Co/Sb intermixing on both sites was refined but did not deviate from the fully ordered model within error. The free *y* coordinate for Li2 was initially fixed to the value from the $Na_3Co_2SbO_6$ starting model,[8] due to the relative insensitivity of XRD data to light Li atoms, and refined in the final cycles. Li2 did not move, within error, from its position in the initial $Na_3Co_2SbO_6$ model. A trace amount of the orthorhombic phase (the structure of which is described below) was included in the refinement. The final Rietveld fit is shown in Figure 1 and the refined structure in Figure 2. Details of the refinement and the refined structure are given in Table 1, with selected bond data including bond valence sums (BVS)[39] in Table 2. The structure is not significantly different to that reported in the parallel work of Stratan et al.,[32] except that they report a small but statistically significant degree of Li/Co intersite mixing and their unit cell at room temperature is slightly smaller (230.610(11) Å^3 vs. 234.02(4) Å^3). These two points of difference may be related and a consequence of the different synthetic routes, but are also within the range of variations commonly seen between refinements using data sets from different instruments. A crystallographic information file (CIF) for the final refined structure is available as Supplementary Information.

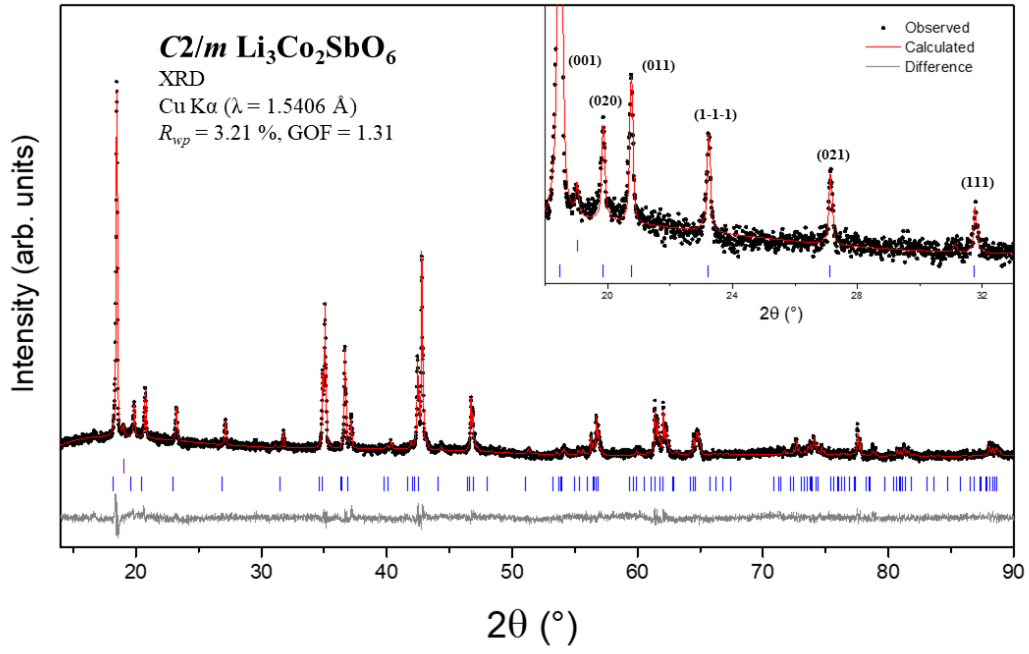

***Figure 1**: Rietveld refinement against XRD data (λ= 1.5406Å) for the C2/m honeycomb phase of $Li_3Co_2SbO_6$ at room temperature. Black circles are experimental data, the red line is*

the calculated pattern and the grey line is the difference. Bragg peaks are indicated by blue tick marks; the upper purple tick mark at 19° indicates the sole observed peak from a trace fraction of the orthorhombic phase. The inset highlights peaks due to Co:Sb honeycomb superlattice ordering, with Miller indices in parentheses.

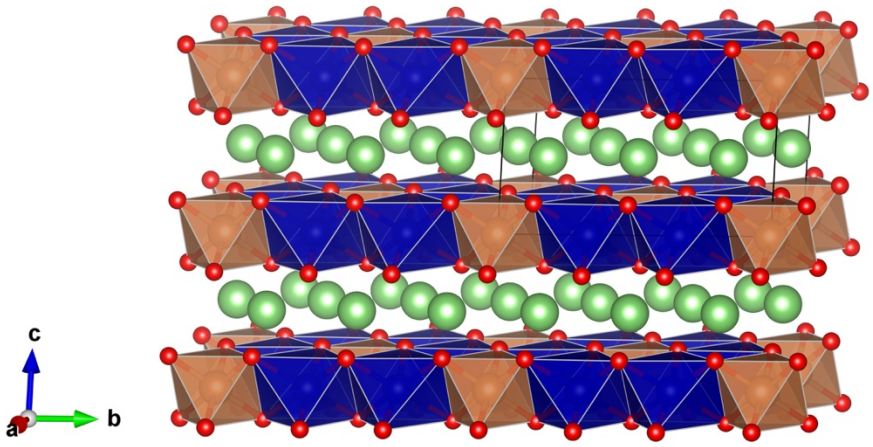

Figure 2 *Crystal structure of the C2/m O3-type honeycomb phase of $Li_3Co_2SbO_6$. CoO_6 octahedra are blue, SbO_6 octahedra are bronze, O atoms are red and Li atoms are green.*

Table 1: Unit cell dimensions, fractional coordinates and isotropic atomic displacement parameters for the honeycomb phase of $Li_3Co_2SbO_6$, from Rietveld-refinement against XRD data. Superscript symbols indicate constraints.

Honeycomb $Li_3Co_2SbO_6$			**Crystal system**			**Space Group**	
GOF = 1.31, R_{wp} = 3.21%			Monoclinic			*C*2/*m*	
Radiation	**T (K)**	**a (Å)**	**b (Å)**	**c (Å)**	**β (°)**	**Volume (Å^3)**	
Cu Kα	298	5.2717(6)	9.0871(10)	5.2039(6)	110.1553(14)	234.02(5)	
Atom	**x**		**y**	**z**	**Occ.**	**B_{iso}(Å^2)**	**Wyckoff**
Co	0		2/3	0	1	0.3(2)	4*g*
Sb	0		0	0	1	0.2(2)	2*a*
O1	0.274(3)		0 348(2)	0.772(5)	1	0.9(4)†	8*j*
O2	0.246(4)		1/2	0.225(9)	1	0.9(4)†	4*i*
Li1	0		1/2	1/2	1	0.5(2)‡	2*d*
Li2	1/2		0.330(9)	1/2	1	0.5(2)‡	4*h*

Table 2: Selected interatomic distances (Å) and bond valence sums (BVS) for the honeycomb phase of $Li_3Co_2SbO_6$ at room temperature.

Co–O1 (x2)	2.138(6)	Li1–O1 (x4)	2.142(8)
Co–O1 (x2)	2.168(14)	Li1–O2 (x2)	2.239(18)
Co–O2 (x2)	2.075(10)	Average	2.17(2)
Average	2.127(18)	BVS (Li1)	0.8
BVS (Co)	1.9	Li2–O1 (x2)	2.147(13)
Sb-O1 (x4)	1.937(6)	Li2–O1 (x2)	2.30(6)
Sb-O2 (x2)	2.059(19)	Li2–O2 (x2)	2.22(6)
Average	1.98(4)	Average	2.22(2)
BVS (Sb)	5.1	BVS (Li2)	0.9

The honeycomb phase of $Li_3Co_2SbO_6$ has a smaller unit cell than that of $Na_3Co_2SbO_6$, with volumes of 234.02(5) and 266.43(18) $Å^3$ respectively. The difference in unit cell dimensions is most pronounced along the layer-stacking *c* axis (5.637(2) and 5.2717(6) Å), consistent with the larger ionic radius of Na^+ vs. Li^+ (1.02 vs. 0.76 Å). The superlattice reflections due to 2:1 Co:Sb honeycomb ordering are sharp, demonstrating the absence of appreciable stacking faults.[22,40,41] Calculated BVS for the cations are all very close to their nominal values, further validating the structural changes from the $Na_3Co_2SbO_6$ starting model.

The orthorhombic phase was indexed in the orthorhombic space group *Fddd* and is isostructural with $Li_3Co_2TaO_6$.[24] For the structural refinements it was assumed that each cation site was fully occupied. B_{iso} values for O1 and O2 diverged slightly, indicating some degree of correlation in the refinement, so were constrained to the same value. The free *z* coordinate for Li1 was initially fixed at the value from the $Li_3Co_2TaO_6$ starting model, due to the relative insensitivity of XRD to light Li atoms,[24] and only refined in the last cycles. Li1 was found to move only slightly from its position in the $Li_3Co_2TaO_6$ model, improving the fit from R_{wp} = 23.57%, GOF = 1.66 to R_{wp} = 22.67%, GOF = 1.59 in the final refinement. The final Rietveld fit is shown in Figure 3 and a representation of the structure in Figure 4. Details of the refinement and the refined structure are given in Table 3, with selected bond data including BVS in Table 4. A CIF for the final refined structure is available as Supplementary Information.

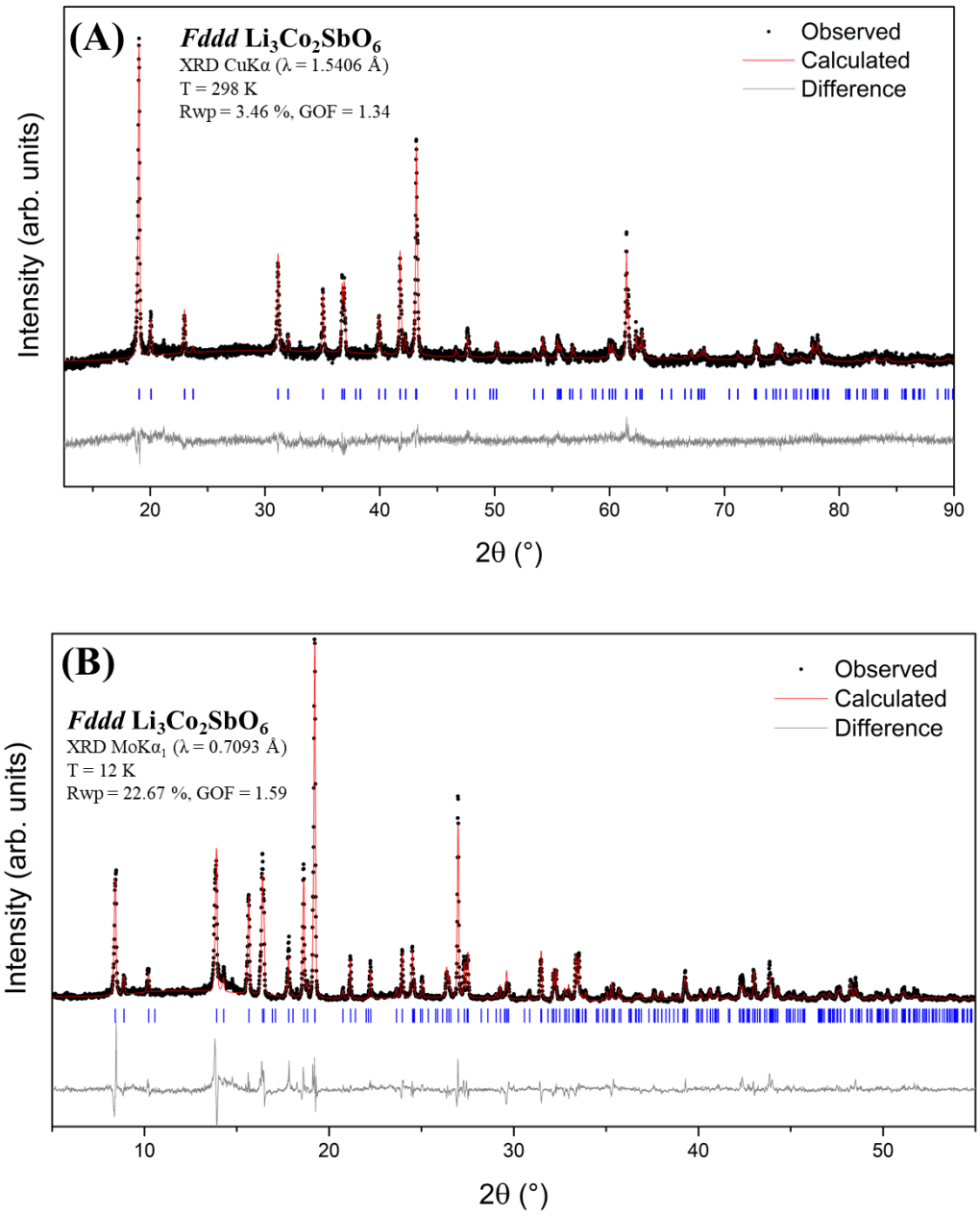

Figure 3: *Rietveld refinement of the orthorhombic Fddd phase of $Li_3Co_2SbO_6$ against XRD data from (A) a Cu Kα source (λ= 1.5418 Å) at 298 K and (B) a Mo $Kα_1$ source (λ= 0.7093 Å) at 12 K under vacuum. Observed data are black circles, the calculated fit is a red line and the difference is a grey line. Blue tick marks indicate Bragg reflections.*

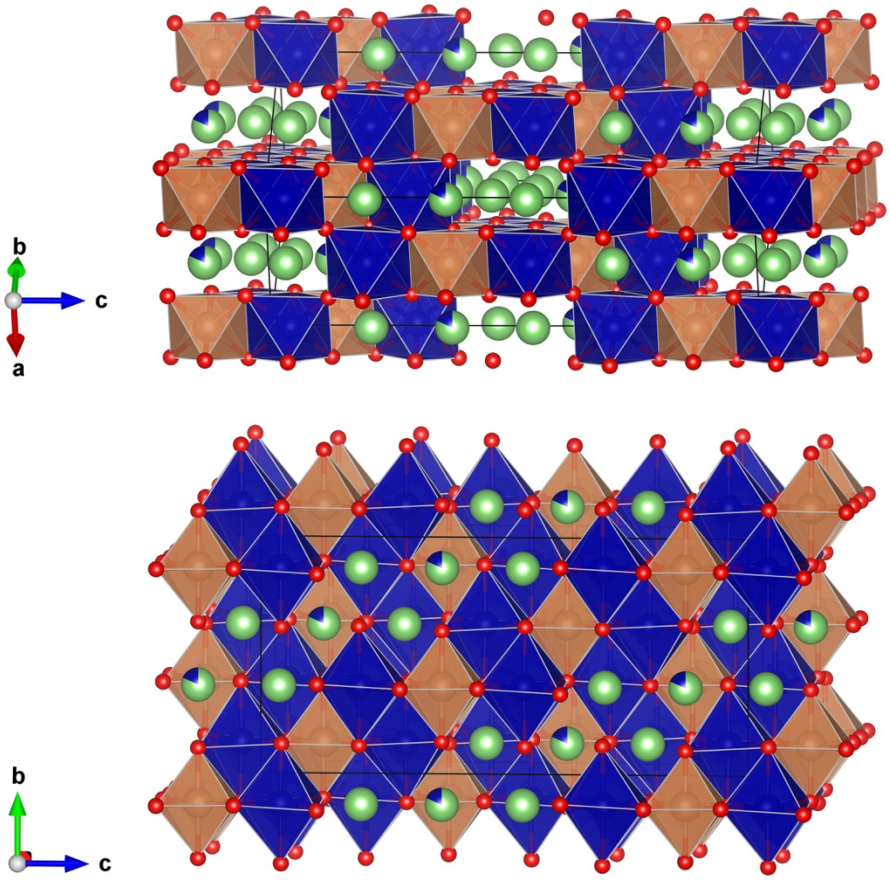

Figure 4 *Crystal structure of the orthorhombic Fddd phase of $Li_3Co_2SbO_6$ in two different orientations. CoO_6 octahedra are blue, SbO_6 octahedra are bronze, O atoms are red and Li atoms are green. Coloured wedges show mixed occupancies.*

Table 3 Unit cell dimensions, fractional coordinates, occupancies and isotropic atomic displacement parameters for the orthorhombic phase of $Li_3Co_2SbO_6$, from Rietveld-refinement against XRD data at 12 K; and unit cell dimensions only (in italics) from Rietveld-refinement against XRD data at 298 K Superscript symbols indicate constraints.

Orthorhombic $Li_3Co_2SbO_6$				**Crystal system**		**Space Group**	
				Orthorhombic		*Fddd*	
Radiation	**T (K)**	**a (Å)**	**b (Å)**	**c (Å)**	**α= β=γ (°)**	**Volume ($Å^3$)**	
Cu Kα	*298*	*5.937(2)*	*8.703(2)*	*17.944(5)*	*90*	*927.4(4)*	
Mo $Kα_1$	12	5.918(2)	8.666(4)	17.884(7)	90	917.1(6)	
Atom		**x**	**y**	**z**	**Occ.**	**B_{iso}($Å^2$)**	**Wyckoff**
Sb		1/8	1/8	1/8	1	0.2(1)	8*a*
Co1		1/8	1/8	0.2934(2)	1	0.3(1)	16*g*
Li1		1/8	5/8	0.2907(2)	1	1.0(4)	16*g*
Li2/Co2		1/8	5/8	1/8	0.82/0.18 (4)	1.0(3)	8*b*
O1		1/8	0.358(2)	1/8	1	0.40(15)†	16*f*
O2		0.1156(17)	0.377(2)	0.2954(7)	1	0.40(15)†	32*h*
GOF = 1.34, R_{wp} = 3.46% (Cu Kα); GOF = 1.59, R_{wp} = 22.67% (Mo $Kα_1$)							

Table 4 Selected interatomic distances (Å) and bond valence sums (BVS) for the orthorhombic phase of $Li_3Co_2SbO_6$ at 12 K.

Co1–O1 (x2)	2.0841(7)	Li1–O1 (x2)	2.118(7)
Co1–O2 (x2)	2.132(7)	Li1–O2 (x2)	2.1506(3)
Co1–O2 (x2)	2.186(3)	Li1–O2(x2)	2.174(7)
Average	2.134(4)	Average	2.15(4)
BVS (Co1)	1.8	BVS (Li2)	0.9
Sb-O1 (x2)	2.014(7)	Co2/Li2–O1 (x2)	2.316(14)
Sb-O2 (x4)	2.017(14)	Co2/Li2–O2 (x4)	2.094(7)
Average	2.016(14)	Average	2.17(5)
BVS (Sb)	4.5	BVS (Co2/Li2)	1.7/0.9

In this orthorhombic phase, SbO_6 octahedra share 12 edges with (Li,Co)O_6 octahedra. Placing Sb on the 8*a* Wykoff site maximises Sb–Sb distances to minimise electrostatic repulsion between Sb^{5+} cations. Li and Co are distributed over three crystallographically independent sites with varying Li:Co contents, all of which were refined. The 8*b* site is the most distorted of these, with the longest *M*-O bond distances, and was mostly occupied by Li with a small refined fraction of Co; while the two 16*g* sites were fully occupied by Co or Li within the

standard deviations of the refinement, and were fixed as such. This is a notable departure from the starting model of $Li_3Co_2TaO_6$, which had Ta on the 8*a* site but a statistical occupancy of all three Li/Co sites.[24] Calculated BVS for the cations are reasonable, all falling within 10% of their nominal values with the exception of the small fraction of Co2 (BVS = 1.7+) on the mixed site dominated by Li2 (BVS = 0.9+). Note that the refined occupancies suggest a slightly Co-rich composition $Li_{2.82(7)}Co_{2.18(7)}SbO_6$. This is consistent with our observations from synthesis that the orthorhombic phase forms slightly Li-rich, but is subsequently susceptible to Li and Sb loss. Nevertheless, given that this non-stoichiometry is only barely statistically significant (and may be compensated for by a degree of Li substitution onto the Co1 site that is too small to be refined), we will continue to refer to the phase as $Li_3Co_2SbO_6$, except where that non-stoichiometry is potentially significant (as in the discussion of magnetic properties, below).

Magnetic properties

Temperature-dependent magnetic susceptibility data for the honeycomb phase of $Li_3Co_2SbO_6$ show an AFM ordering transition at a Néel temperature T_N = 14 K (Figure 5). There was no significant divergence between data collected under zero field-cooled (ZFC) and field-cooled (FC) conditions using an applied field of 0.1 T. A Curie-Weiss fit to ZFC data over the range 150-300 K yielded a Weiss constant θ_w = 18.1 K and an effective magnetic moment of μ_{eff} = 5.04 μ_B per Co^{2+} ion. The latter value is consistent with high-spin Co^{2+} (d^7, S=3/2, μ_{so} = 3.87 μ_B), with an unquenched orbital contribution in a $^4T_{1g}$ (using the octahedral notation) ground state, and is comparable to μ_{eff} = 5.22 μ_B reported for $Na_3Co_2SbO_6$.[8] The small deviation in susceptibility observed around 75-80 K is due to a trace amount of the orthorhombic phase (the magnetic properties of which are described below). The values T_N = 14 K, θ_w = 18.1 K for $Li_3Co_2SbO_6$ can be compared to θ_w = 8 K and T_N = 15 K for $Li_3Ni_2SbO_6$,[9] and T_N = 8.3 K, θ_w = 2.2 K for $Na_3Co_2SbO_6$. In all cases, the positive Weiss constants θ_w indicate the presence of significant ferromagnetic contributions above the AFM transition temperature.

The magnetic constants are slightly different to those reported in the parallel work of Stratan et al.,[32] who obtained lower values for T_N (9.9 K), θ_w (14 K) and μ_{eff} (3.3 μ_B per Co^{2+} ion). This suggests that the solid-state precursor synthetic route produces a slightly better-ordered sample than the ion-exchange route, as would be expected. However, the qualitative behaviour is the clearly the same and the Weiss constant is positive in both cases.

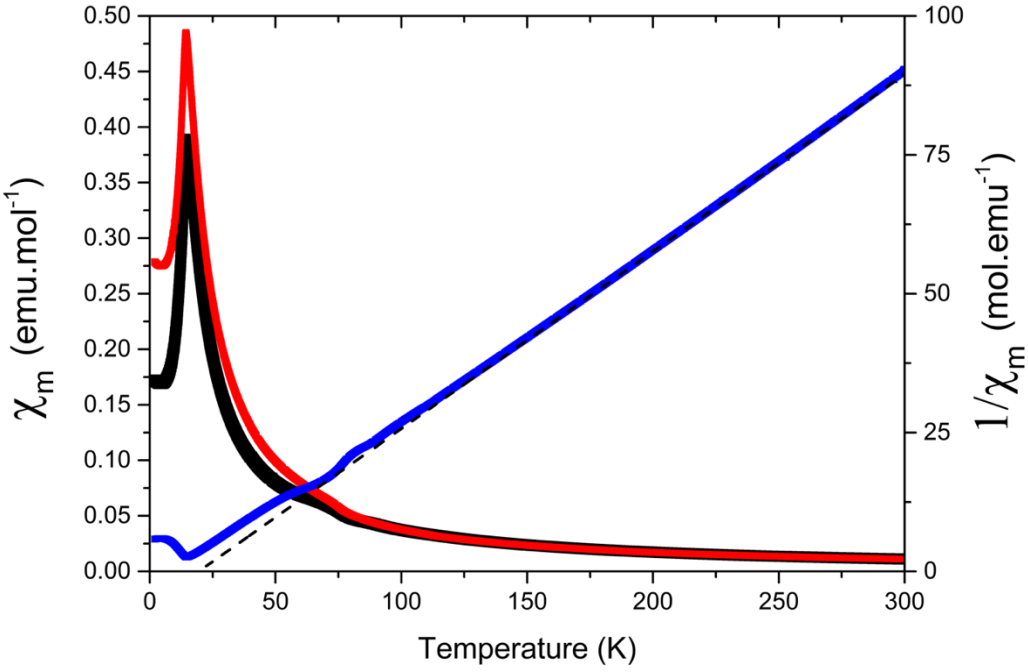

***Figure 5**: Temperature-dependent DC magnetic susceptibility (χ_m) and inverse magnetic susceptibility ($1/\chi_m$) as functions of temperature for the honeycomb phase of $Li_3Co_2SbO_6$, using an applied field of 0.1 T. The ZFC curve is black, the FC curve is red, and the inverse susceptibility is blue. The dotted black line shows the Curie-Weiss fit to the ZFC inverse susceptibility.*

Field-dependent magnetisation data for the honeycomb phase of $Li_3Co_2SbO_6$ were collected over the field range -3 T ≤ H ≤ 3 T (Figure 6). At T = 20 K (above T_N), the behaviour is close to linear. At 2 K (below T_N), a metamagnetic transition is apparent at H = ~ 0.7 T. Other honeycomb oxides have been reported to undergo similar field-induced transitions, e.g.: $Na_3Co_2SbO_6$ has a magnetisation shoulder above H = 1 T, which has been attributed to a field-induced spin-flop transition;[8,13] $Na_2Co_2TeO_6$ has an upturn in magnetisation at ~5 T;[13,29,42] and $Na_3Ni_2BiO_6$ shows evidence of transition(s) from 4-7 T depending on measurement temperature.[17] These results collectively underline the finely balanced and competing/frustrated nature of magnetic exchange in honeycomb antiferromagnets. Again, the field-dependent magnetisation of honeycomb $Li_3Co_2SbO_6$ is qualitatively the same as that reported in the parallel work of Stratan et al.,[32] leading to the same conclusion of a probable spin-flop transition.

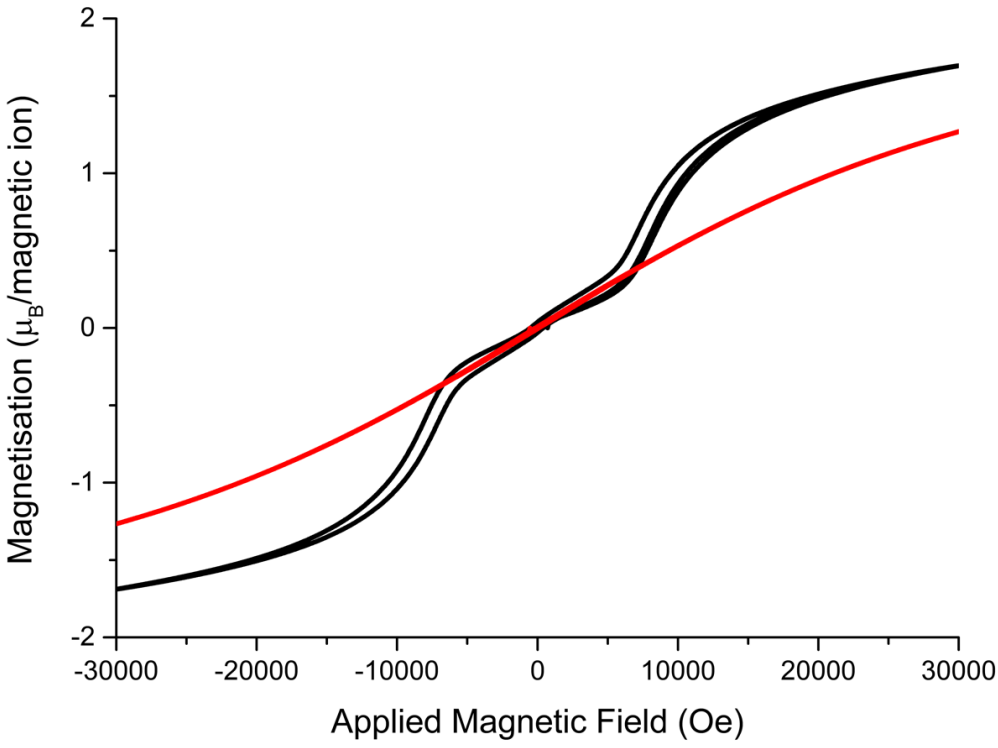

Figure 6: *Field-dependent magnetisation of the honeycomb phase of $Li_3Co_2SbO_6$ at 2 K (black) and 20 K (red), below and above T_N = 14.5 K, respectively.*

Temperature-dependent magnetic susceptibility data for the orthorhombic phase of $Li_3Co_2SbO_6$ under ZFC conditions show a pronounced AFM transition on cooling through T_N = 113 K followed by more transitions at 80 K and 60 K (Figure 7). Noting that no impurity phases were evident in XRD data, the series of transitions suggests close competition between at least three ground states in this compound. A Curie-Weiss fit to the ZFC data for T > 160 K yields μ_{eff} = 5.06 μ_B, slightly larger than for the honeycomb phase of $Li_3Co_2SbO_6$; while if the slight refined non-stoichiometry of the sample, $Li_{2.82}Co_{2.18}SbO_6$, is correct, the expected spin-only moment μ_{so} would be reduced from μ_{so} = 3.87 to 3.78 μ_B due to the presence of some reduced Co^{1+}. Regardless, there are significant contributions from an unquenched orbital component, as is typical for HS Co^{2+} oxides. The highly negative Weiss constant θ_w = -181 K indicates dominant AFM exchange. The FC data strongly diverge from the ZFC data below T_N, with the applied field of 0.1 T appearing to be sufficient to induce an FM state.

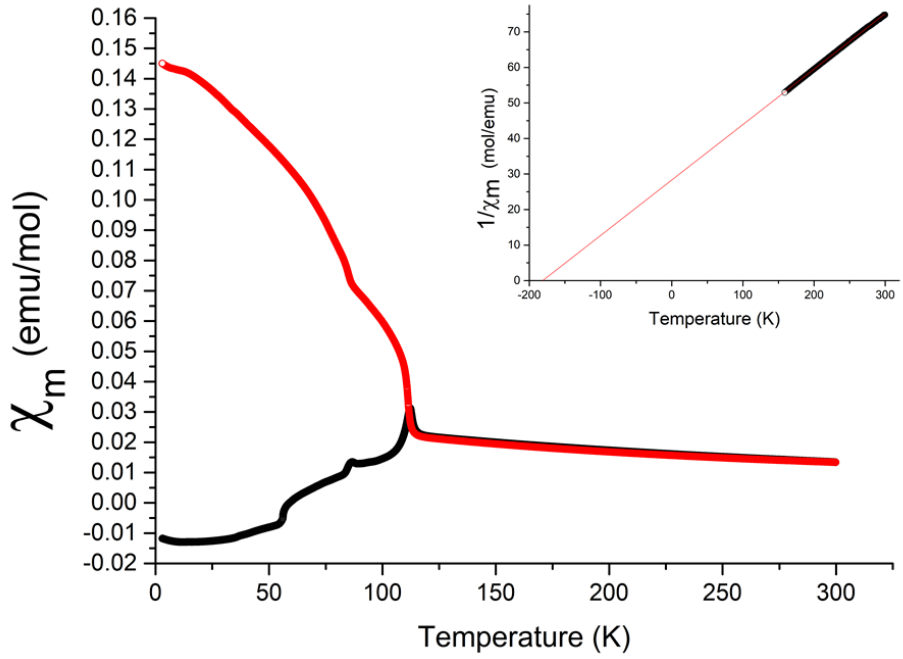

Figure 7: *Magnetic susceptibility as a function of temperature for the orthorhombic phase of $Li_3Co_2SbO_6$ in an applied field of 0.1 T. ZFC data are black and FC data are red. The inset shows the Curie-Weiss fit to ZFC inverse susceptibility above 160 K.*

Field-dependent magnetisation data for the orthorhombic phase of $Li_3Co_2SbO_6$ were collected over a field range -3 T ≤ H ≤ 3 T (Figure 8) at T = 2 K and 90 K. Both data sets show predominantly AFM behaviour with a narrow hysteresis opening, but only the 2 K data show a (small) remanent magnetisation. The magnetisation is approximately two orders of magnitude smaller than for the honeycomb phase at the same fields.

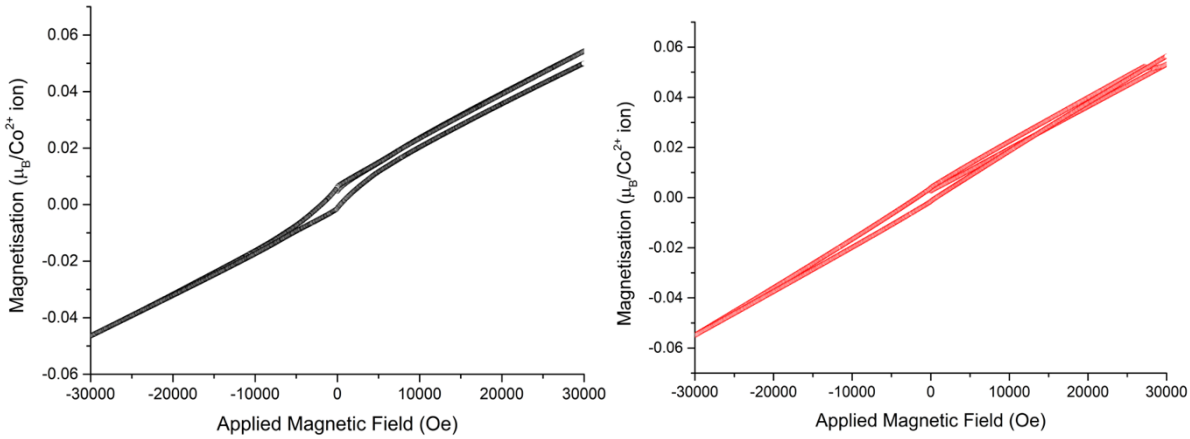

Figure 8: *Field-dependent magnetisation data for the orthorhombic phase of $Li_3Co_2SbO_6$ at 2 K (black) and 90 K (red).*

Low-temperature neutron diffraction data

NPD data for the honeycomb phase of $Li_3Co_2SbO_6$ at 3 K (below T_N) vs. 20 K (above T_N) revealed magnetic Bragg peaks that could be indexed to a propagation vector **k** = (0 0 ½). Representational analysis unambigiously led to the best fit being obtained for the same irreducible representation (irrep), Γ_1, found in the parallel work of Stratan et al.[32] The analysis procedure and table of basis vectors are identical to those reported in that work, and are therefore not reproduced here. The Γ_1 irrep corresponds to the magnetic space group C_c2/m, which has ferromagnetic (FM) honeycomb planes with AFM coupling between them. This so-called A-type AFM structure has not previously been observed in the honeycomb phases. The spins are oriented along the *b* axis. The final Rietveld fit is shown in Figure 9, yielding a refined magnetic moment of 2.53(3) μ_B/Co along *b* at 3 K, close to the fully ordered value of 3 μ_B/Co for HS Co^{2+}. Note that Stratan et al.[32] report M = 3.74(4) μ_B/Co at 1.5 K, or 1.75(2) μ_B/Co along *b*. This is consistent with the magnetometry results discussed above, which indicate a slightly better-ordered sample from solid-state precursor synthesis compared to ion-exchange synthesis.

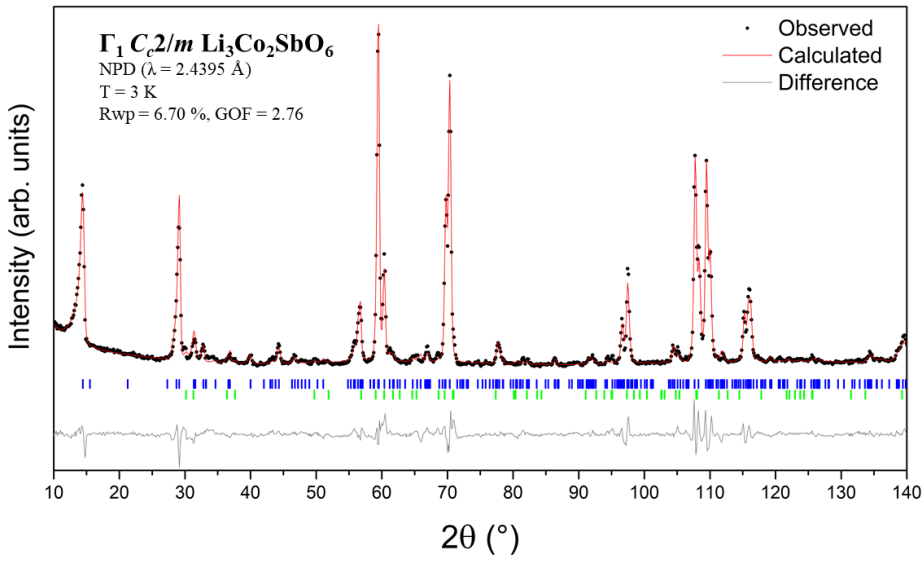

Figure 9: *Rietveld fit to 3 K NPD data (λ = 2.4395 Å) for the honeycomb phase of $Li_3Co_2SbO_6$ using the nuclear plus Γ_1 (C_c2/m) magnetic model. Black circles are the observed diffraction pattern, the red line is the calculated pattern and the grey line gives the difference profile. Blue ticks mark reflections for the magnetic and nuclear peak positions. Green ticks are a minor orthorhombic $Li_3Co_2SbO_6$ impurity.*

While the A-type AFM state has not previously been observed for a $A_xM_2M'O_6$ honeycomb phase, it is interesting to note that this state was originally predicted for the honeycomb phase of $Li_3Ni_2SbO_6$ [9] prior to NPD experiments that showed it has a zig-zag ground state. The Ni-O-Ni magnetic exchange pathway in this compound is ~90°, which is expected to yield FM in-plane interactions based on Goodenough-Kanamori rules. A positive Weiss temperature (θ = 8 K) supported this prediction, so the onset of long-range AFM below T_N = 15 K was assumed to be due to AFM inter-layer coupling. The Co analogue reported here has an almost identical Néel temperature, Weiss temperature, and *M*-O-*M* bond angle – but in this case A-type AFM is indeed the resulting ground state. The biggest difference between these compounds is their electronic ground state: Ni^{2+} is d^8, which in octahedral coordination has a $^3A_{2g}$ ground term with filled t_{2g} orbitals; while Co^{2+} is d^7, with a $^4T_{1g}$ ground term and an unpaired electron in one t_{2g} orbital. This additional unpaired electron contributes additional unquenched angular orbital momenta, which may be a factor in the emergence of A-type ordering.

Considering the magnetic structure of honeycomb $Li_3Co_2SbO_6$, the spin-flop transition observed in field-dependent magnetisation data (Figure 6) almost certainly corresponds to a change from AFM to FM interactions between the FM planes: i.e., a change from A-type AFM (magnetic space group C_c2/m) to 3-D FM (magnetic space group $C2/m$). In order to test this, we collected field-dependent NPD data between 0 and 6 T at 1.8 K. The data are shown in Figure 10. The characteristic A-type AFM Bragg peaks disappear as the field is increased, while the (0 0 *l*) nuclear reflections (perpendicular to the honeycomb planes) show the strongest growth in intensity. Unfortunately, complex preferred orientation due to partial particle reorientation in the field meant that we were unable to refine the magnetic structure to obtain a precise value and orientation for the ordered moment at 6 T (note that the (-3 3 1) nuclear reflection, equivalent to (1 1 0) in the hexagonal parent phase, i.e., parallel to the honeycomb planes, weakens as the field increases). Nevertheless, these intensity trends confirm a metamagnetic transition at high fields to an in-plane 3-D FM state.

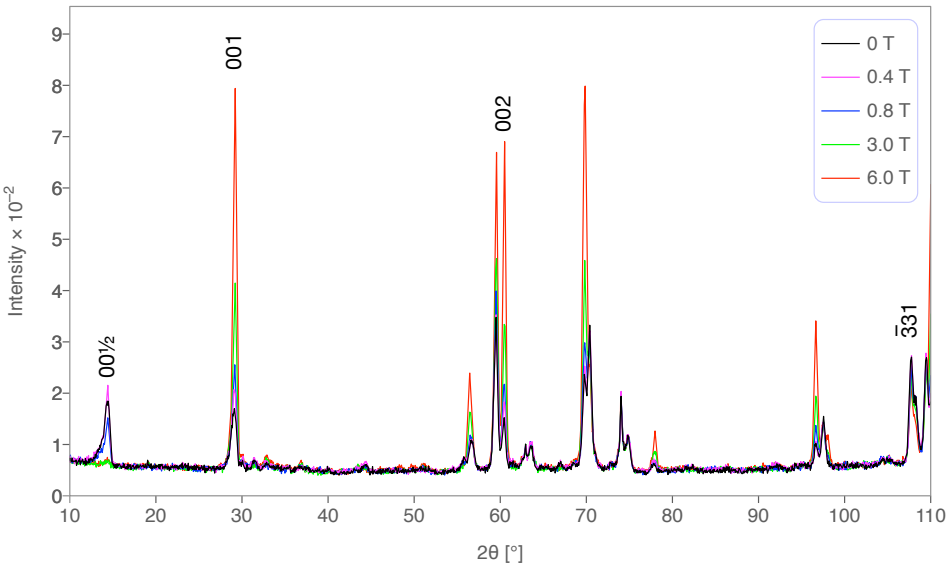

Figure 10: *NPD data (λ = 2.4395 Å) for the honeycomb phase of $Li_3Co_2SbO_6$ at 1.8 K in increasing magnetic fields. Note that the doublets at 63° and 74.5° are Al peaks from the front and back side of the cryomagnet bore.*

NPD data for the orthorhombic phase of $Li_3Co_2SbO_6$ at 125 K (above T_N) and 3 K are shown in Figure 11. The difference between them highlights the magnetic Bragg peaks, proving that this phase undergoes long-range spin ordering. However, the majority could not be indexed with a rational **k**-vector, indicating that the ground-state is incommensurate. A **k**-vector search failed to identify a convincing result due to an insufficient number of observed magnetic peaks relative to the nuclear symmetry. Further insights into the magnetic structure of the orthorhombic phase of $Li_3Co_2SbO_6$ will require single-crystal and/or polarised neutron diffraction experiments to obtain more unambiguous observed magnetic peaks.

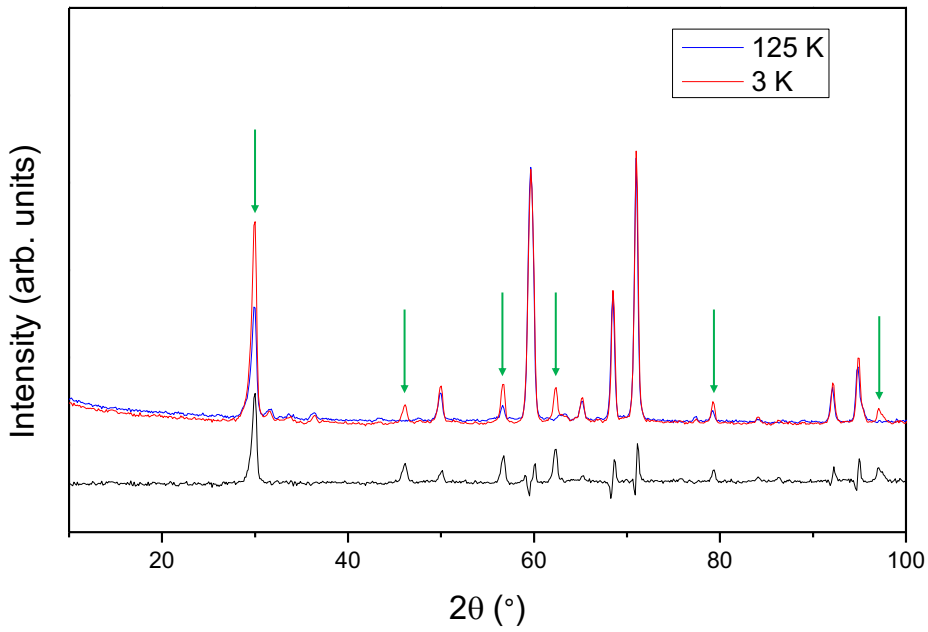

Figure 11: *NPD data (λ = 2.4395 Å) of orthorhombic $Li_3Co_2SbO_6$ at 3 K (red) and 125 K (blue). The difference curve (black) shows the possible magnetic Bragg peaks, highlighted with green arrows.*

Electrochemical properties

The honeycomb and orthorhombic phases of $Li_3Co_2SbO_6$ were both tested as active positive electrode (cathode) materials in Li-ion coin cell batteries. Charge and discharge cycles are shown in Figures 12 and 13. Upon the first charge to 4.2 V, the honeycomb phase has a capacity of 32 mAh/g, while the orthorhombic phase has a capacity of 20 mAh/g. These low capacities fade after the first cycle, to 3.4 mAh/g and 3.7 mAh/g, respectively, and continue to decrease with each subsequent cycle. Note that the stoichiometry $Li_3Co_2SbO_6$ gives a calculated theoretical capacity of 75.2 mAh/g based on Co^{2+}/Co^{3+} redox alone, at which point 2/3 of the Li has been removed.

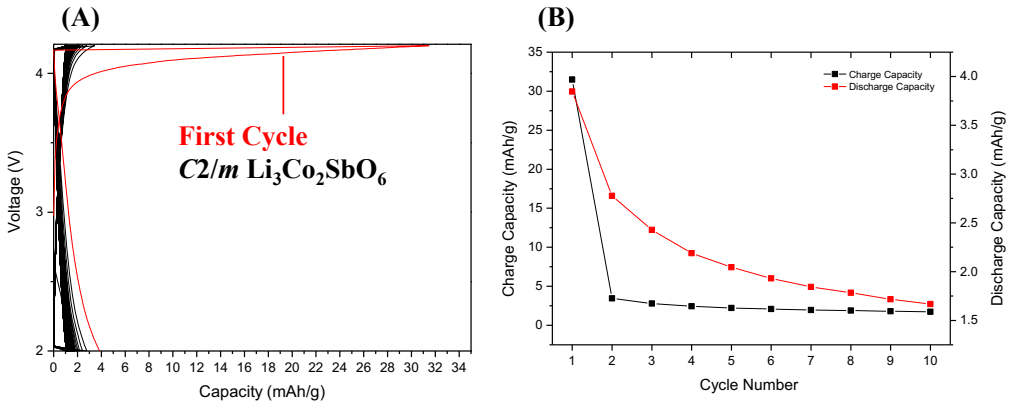

Figure 12 *(A) Charge/discharge voltage profiles of honeycomb-type $Li_3Co_2SbO_6$, with the first cycle in red and the next 99 cycles in black. (B) Capacity retention of charge (black) and discharge (red) for the first 10 cycles.*

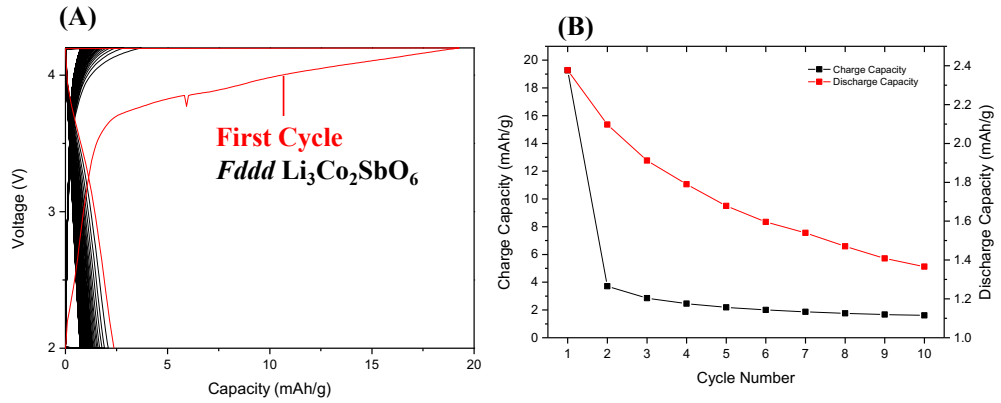

Figure 13: *(A) Charge/discharge voltage profiles for the orthorhombic phase of $Li_3Co_2SbO_6$, with the first cycle in red and the next 99 cycles in black. (B) Capacity retention of charge (black) and discharge (red) for the first 10 cycles.*

The capacity is inferior to a number of other honeycomb oxides, notably the Ni compounds. For example, $Na_3Ni_2SbO_6$ has been shown to have reversible capacities between 110-130 mAh/g with 70% retention over 500 cycles.[43,44] Similarly, $Na_2Ni_2TeO_6$ reversible capacity of 110 mAh/g.[45] Of the Li compounds, Li_4NiTeO_6 has a reversible capacity of 110-120 mAh/g.[46,47] However, the closest analogue to $Li_3Co_2SbO_6$ for which electrochemical data have been reported, $Li_3Ni_2BiO_6$, has a similarly low capacity of 22 mAh/g.[48]

Conclusions

We have shown that $Li_3Co_2SbO_6$ can be prepared by conventional solid-state synthesis from pre-prepared Li_3SbO_4 and CoO. These precursor phases were found to be necessary so that Sb and Co would be present in their desired oxidation states (Sb^{5+} and Co^{2+}, at the upper and lower ends of their normal ranges in oxides, respectively) prior to high-temperature reaction under a protective Ar flow. Two distinct phases can be obtained by controlling particle size, initial lithium excess, and reaction time. Conventional grinding, stoichiometric reagents and short reaction times yield a layered honeycomb phase isostructural with $Na_3Co_2SbO_6$; while ball-milling, a slight Li excess, and longer reaction times yield an *Fddd* orthorhombic phase isostructural with $Li_3Co_2TaO_6$ but with much more well-defined Li/Co ordering. Both phases are challenging to make as pure samples, with very narrow ranges of thermodynamic stability between the minimum required synthesis temperature and decomposition due to evaporative loss of Li and/or Sb. Future work using low-temperature *chimie douce* synthetic routes may help address these challenges, but at the expense of crystallinity, which was the priority in the present work aimed at solving and refining the fully ordered structures.

Neither phase shows promising electrochemical performance as lithium-ion battery cathode in their as-made states, although it may be possible to improve this in the future by ball-milling to micron scale before casting onto Al foil, to increase surface area. The poor performance might be due to irreversible structural changes, which could potentially be explored through future *in situ* diffraction studies and/or *ex situ* studies of charged samples.

Both phases show complex and interesting low-temperature magnetism. Below T_N = 14 K, the layered honeycomb phase adopts A-type AFM order (FM planes, AFM coupled), which has been predicted but not previously observed for any $A_xM_2M'O_6$ honeycomb phase. Isothermal magnetisation and in-field NPD below T_N reveal a metamagnetic "spin-flop" transition to a 3-D FM phase above H ~ 0.7 T.

The orthorhombic phase also undergoes long-range AFM order, at the significantly higher T_N = 112 K, but in this case with a strongly negative Weiss constant θ_w = -181 K that points to somewhat frustrated AFM intersections in paramagnetic regime. At lower temperatures, it undergoes two more transitions at 80 K and 60, suggesting at least three competing ground states. Strong FC/ZFC divergence, and soft hysteresis in isothermal magnetisation, below T_N suggest a fine balance between local AFM and FM exchange interactions. Low-tempertaure NPD data point to an incommensurate AFM ground state, which could not be confidently indexed based on the limited number of observed reflections. Further detailed measurements

(preferably on single crystals, which are not presently available) will be required to unravel this complex behaviour.

Supplementary Information

Crystallographic information files (CIFs) for the final refined structures of $Li_3Co_2SbO_6$ have been deposited with the Cambridge Structural Database (CSD), deposition numbers 1937387 (honeycomb phase) and 1937386 (orthorhombic phase).

Acknowledgements

CDL and BJK received funding for this work from the Australian Research Council – Discovery Projects. AJB received funding from the Australian Institute for Nuclear Science and Engineering – AINSE Honours Scholarships.

References

(1) Delmas, C.; Fouassier, C.; Hagenmuller, P. Structural Classification and Properties of the Layered Oxides. *Phys. BC* **1980**, *99* (1–4), 81–85.

(2) Delmas, C.; Braconnier, J.; Fouassier, C.; Hagenmuller, P. Electrochemical Intercalation of Sodium in Na_xCoO_2 Bronzes. *Solid State Ion.* **1981**, *3–4*, 165–169.

(3) Berthelot, R.; Carlier, D.; Delmas, C. Electrochemical Investigation of the P2–Na x CoO_2 Phase Diagram. *Nat. Mater.* **2011**, *10* (1), 74–80.

(4) Shacklette, L. W. Rechargeable Electrodes from Sodium Cobalt Bronzes. *J. Electrochem. Soc.* **1988**, *135* (11), 2669.

(5) Takada, K.; Sakurai, H.; Takayama-Muromachi, E.; Izumi, F.; Dilanian, R. A.; Sasaki, T. Superconductivity in Two-Dimensional CoO_2 Layers. *Nature* **2003**, *422* (6927), 53–55.

(6) Greaves, C.; Katib, S. M. A. The Structural Chemistry of $Li_3Zn_2MO_6$ (M=Sb, Bi) and Related Phases. *Mater. Res. Bull.* **1990**, *25* (9), 1175–1182.

(7) Seibel, E. M.; Roudebush, J. H.; Ali, M. N.; Ross, K. A.; Cava, R. J. Structure and Magnetic Properties of the Spin-1/2-Based Honeycomb $NaNi_2BiO_{6-\delta}$ and Its Hydrate $NaNi_2BiO_{6-\delta} \cdot 1.7H_2O$. *Inorg. Chem.* **2014**, *53* (20), 10989–10995.

(8) Wong, C.; Avdeev, M.; Ling, C. D. Zig-Zag Magnetic Ordering in Honeycomb-Layered $Na_3Co_2SbO_6$. *J. Solid State Chem.* **2016**, *243*, 18–22.

(9) Zvereva, E. A.; Evstigneeva, M. A.; Nalbandyan, V. B.; Savelieva, O. A.; Ibragimov, S. A.; Volkova, O. S.; Medvedeva, L. I.; Vasiliev, A. N.; Klingeler, R.; Buechner, B. Monoclinic Honeycomb-Layered Compound $Li_3Ni_2SbO_6$: Preparation, Crystal Structure and Magnetic Properties. *Dalton Trans.* **2011**, *41* (2), 572–580.

(10) Zhong, J.; Chen, X.; Chen, D.; Liu, M.; Zhu, Y.; Li, X.; Ji, Z. A Novel Rare-Earth Free Red-Emitting $Li_3Mg_2SbO_6$:Mn4+ Phosphor-in-Glass for Warm w-LEDs: Synthesis, Structure, and Luminescence Properties. *J. Alloys Compd.* **2019**, *773*, 413–422.

(11) Yuan, D.; Liang, X.; Wu, L.; Cao, Y.; Ai, X.; Feng, J.; Yang, H. A Honeycomb-Layered $Na_3Ni_2SbO_6$: A High-Rate and Cycle-Stable Cathode for Sodium-Ion Batteries. *Adv. Mater.* **2014**, *26* (36), 6301–6306.

(12) Xu, J.; Assoud, A.; Soheilnia, N.; Derakhshan, S.; Cuthbert, H. L.; Greedan, J. E.; Whangbo, M. H.; Kleinke, H. Synthesis, Structure, and Magnetic Properties of the Layered Copper(II) Oxide $Na_2Cu_2TeO_6$. *Inorg. Chem.* **2005**, *44* (14), 5042–5046.

(13) Viciu, L.; Huang, Q.; Morosan, E.; Zandbergen, H. W.; Greenbaum, N. I.; McQueen, T.; Cava, R. J. Structure and Basic Magnetic Properties of the Honeycomb Lattice Compounds $Na_2Co_2TeO_6$ and $Na_3Co_2SbO_6$. *J. Solid State Chem.* **2007**, *180* (3), 1060–1067.

(14) Uma, S.; Gupta, A. Synthesis and Characterization of New Rocksalt Superstructure Type Layered Oxides $Li_{4.5}M_{0.5}TeO_6$ (M(III)=Cr, Mn, Al, Ga). *Mater. Res. Bull.* **2016**, *76*, 118–123.

(15) Smirnova, O. A.; Nalbandyan, V. B.; Petrenko, A. A.; Avdeev, M. Subsolidus Phase Relations in Na_2O–CuO–Sb_2O_n System and Crystal Structure of New Sodium Copper Antimonate $Na_3Cu_2SbO_6$. *J. Solid State Chem.* **2005**, *178* (4), 1165–1170.

(16) Skakle, J. M. S.; Castellanos R., M. A.; Tovar, S. T.; West, A. R. Synthesis of $Li_3Cu_2SbO_6$, a New Partially Ordered Rock Salt Structure. *J. Solid State Chem.* **1997**, *131* (1), 115–120.

(17) Seibel, E. M.; Roudebush, J. H.; Wu, H.; Huang, Q.; Ali, M. N.; Ji, H.; Cava, R. J. Structure and Magnetic Properties of the A-$NaFeO_2$-Type Honeycomb Compound $Na_3Ni_2BiO_6$. *Inorg. Chem.* **2013**, *52* (23), 13605–13611.

(18) Nalbandyan, V. B.; Avdeev, M.; Evstigneeva, M. A. Crystal Structure of Li_4ZnTeO_6 and Revision of $Li_3Cu_2SbO_6$. *J. Solid State Chem.* **2013**, *199*, 62–65.

(19) Kumar, V.; Gupta, A.; Uma, S. Formation of Honeycomb Ordered Monoclinic $Li_2M_2TeO_6$ (M = Cu, Ni) and Disordered Orthorhombic $Li_2Ni_2TeO_6$ Oxides. *Dalton Trans.* **2013**, *42* (42), 14992–14998.

(20) Kumar, V.; Bhardwaj, N.; Tomar, N.; Thakral, V.; Uma, S. Novel Lithium-Containing Honeycomb Structures. *Inorg. Chem.* **2012**, *51* (20), 10471–10473.

(21) Deng, Z.; Gu, J.; Li, Y.; Li, S.; Peng, J.; Li, X.; Luo, J.; Huang, Y.; Fang, C.; Li, Q.; et al. Ca-Doped $Na_2Zn_2TeO_6$ Layered Sodium Conductor for All-Solid-State Sodium-Ion Batteries. *Electrochimica Acta* **2019**, *298*, 121–126.

(22) Berthelot, R.; Schmidt, W.; Muir, S.; Eilertsen, J.; Etienne, L.; Sleight, A. W.; Subramanian, M. A. New Layered Compounds with Honeycomb Ordering: $Li_3Ni_2BiO_6$, $Li_3NiM'BiO_6$ (M′ = Mg, Cu, Zn), and the Delafossite $Ag_3Ni_2BiO_6$. *Inorg. Chem.* **2012**, *51* (9), 5377–5385.

(23) Berthelot, R.; Schmidt, W.; Sleight, A. W.; Subramanian, M. A. Studies on Solid Solutions Based on Layered Honeycomb-Ordered Phases P2-$Na_2M_2TeO_6$ (M=Co, Ni, Zn). *J. Solid State Chem.* **2012**, *196*, 225–231.

(24) Mather, G. C.; Smith, R. I.; Skakle, J. M. S.; Fletcher, J. G.; R, M. A. C.; Gutierrez, M. P.; West, A. R. Synthesis and Structures of the Partially Ordered Rock Salt Phases, $Li_3M_2XO_6$: M=Mg, Co, Ni; X=Nb, Ta, Sb. *J. Mater. Chem.* **1995**, *5* (8), 1177–1182.

(25) Fletcher, J. G.; Mather, G. C.; West, A. R.; Castellanos, M.; Gutierrez, M. P. $Li_3Ni_2TaO_6$: A Novel Rock Salt Superstructure Phase with Partial Cation Order. *J. Mater. Chem.* **1994**, *4* (8), 1303–1305.

(26) Mather, G. C.; Dussarrat, C.; Etourneau, J.; West, A. R. A Review of Cation-Ordered Rock Salt Superstructureoxides. *J. Mater. Chem.* **2000**, *10* (10), 2219–2230.

(27) Heymann, G.; Selb, E.; Kogler, M.; Götsch, T.; Köck, E.-M.; Penner, S.; Tribus, M.; Janka, O. $Li_3Co_{1.06(1)}TeO_6$: Synthesis, Single-Crystal Structure and Physical Properties of a New Tellurate Compound with CoII/CoIII Mixed Valence and Orthogonally Oriented Li-Ion Channels. *Dalton Trans.* **2017**, *46* (37), 12663–12674.

(28) Masese, T.; Yoshii, K.; Yamaguchi, Y.; Okumura, T.; Huang, Z.-D.; Kato, M.; Kubota, K.; Furutani, J.; Orikasa, Y.; Senoh, H.; et al. Rechargeable Potassium-Ion Batteries with Honeycomb-Layered Tellurates as High Voltage Cathodes and Fast Potassium-Ion Conductors. *Nat. Commun.* **2018**, *9* (1), 3823.

(29) Bera, A. K.; Yusuf, S. M.; Kumar, A.; Ritter, C. Zigzag Antiferromagnetic Ground State with Anisotropic Correlation Lengths in the Quasi-Two-Dimensional Honeycomb Lattice Compound $Na_2Co_2TeO_6$. *Phys. Rev. B* **2017**, *95* (9), 094424.

(30) Liu, H.; Khaliullin, G. Pseudospin Exchange Interactions in d^7 Cobalt Compounds: Possible Realization of the Kitaev Model. *Phys. Rev. B* **2018**, *97* (1), 014407.

(31) Ermolov, A. S., Zvereva, E. A., Stratan, M. I., Nalbandyan, V. B., Evstigneeva, M., Vasiliev, A. N. Static and dynamic magnetic properties of new layered antimonate of lithium and cobalt. Proceedings of the XVI International Youth Scientific School, Kazan Federal University (2013). http://www.mrschool.kpfu.ru/proceedings/mrschool2013.pdf#page=41

(32) Stratan, M.I., Shukaev, I., Vasilchikova, T.M., Vasiliev, A., Korshunov, A., Kurbakov, A., Nalbandyan, V.B., Zvereva, E.A. Synthesis, structure and magnetic properties of honeycomb-layered $Li_3Co_2SbO_6$ with new data on its sodium precursor, $Na_3Co_2SbO_6$. *New Journal of Chemistry* **2019**, in press, available online. https://doi.org/10.1039/c9nj03627j

(33) Skakle, J. M. S.; R, M. A. C.; Tovar, S. T.; Fray, S. M.; West, A. R. The Crystal Structure of Li_3SbO_4. *J. Mater. Chem.* **1996**, *6* (12), 1939–1942.

(34) Blasse, G. New Types of Cation-Order in the Rocksalt Lattice: The Structure of Li_3SbO_4 and Li_3NbO_4. *Z. Für Anorg. Allg. Chem.* **1963**, *326* (1–2), 44–46.

(35) Järvinen, M. Application of Symmetrized Harmonics Expansion to Correction of the Preferred Orientation Effect. *J. Appl. Crystallogr.* **1993**, *26* (4), 525–531.

(36) Coelho, A. A. TOPAS and TOPAS-Academic: An Optimization Program Integrating Computer Algebra and Crystallographic Objects Written in C++. *J. Appl. Crystallogr.* **2018**, *51* (1), 210–218.

(37) Avdeev, M.; Hester, J. R., Echidna: A Decade of High-Resolution Neutron Powder Diffraction at Opal. *J. Appl. Crystallogr.* **2018**, *51*, 1597-1604.

(38) Campbell, B. J.; Stokes, H. T.; Tanner, D. E.; Hatch, D. M., Isodisplace: A Web-Based Tool for Exploring Structural Distortions. *J. Appl. Crystallogr.* **2006**, *39*, 607-614.

(39) Brese, N. E.; O'keeffe, M. Bond-Valence Parameters for Solids. *Acta Crystallogr. B* **1991**, *47* (2), 192–197.

(40) Liu, J.; Yin, L.; Wu, L.; Bai, J.; Bak, S.-M.; Yu, X.; Zhu, Y.; Yang, X.-Q.; Khalifah, P. G. Quantification of Honeycomb Number-Type Stacking Faults: Application to $Na_3Ni_2BiO_6$ Cathodes for Na-Ion Batteries. *Inorg. Chem.* **2016**, *55* (17), 8478–8492.

(41) Shunmugasundaram, R.; Arumugam, R. S.; Dahn, J. R. A Study of Stacking Faults and Superlattice Ordering in Some Li-Rich Layered Transition Metal Oxide Positive Electrode Materials. *J. Electrochem. Soc.* **2016**, *163* (7), A1394–A1400.

(42) Lefrançois, E.; Songvilay, M.; Robert, J.; Nataf, G.; Jordan, E.; Chaix, L.; Colin, C. V.; Lejay, P.; Hadj-Azzem, A.; Ballou, R.; et al. Magnetic Properties of the Honeycomb Oxide $Na_2Co_2TeO_6$. *Phys. Rev. B* **2016**, *94* (21), 214416.

(43) Yuan, D.; Liang, X.; Wu, L.; Cao, Y.; Ai, X.; Feng, J.; Yang, H. A Honeycomb-Layered $Na_3Ni_2SbO_6$: A High-Rate and Cycle-Stable Cathode for Sodium-Ion Batteries. *Adv. Mater.* **2014**, *26* (36), 6301–6306.

(44) Ma, J.; Bo, S.-H.; Wu, L.; Zhu, Y.; Grey, C. P.; Khalifah, P. G. Ordered and Disordered Polymorphs of $Na(Ni_{2/3}Sb_{1/3})O_2$: Honeycomb-Ordered Cathodes for Na-Ion Batteries. *Chem. Mater.* **2015**, *27* (7), 2387–2399.

(45) Gupta, A.; Buddie Mullins, C.; Goodenough, J. B. $Na_2Ni_2TeO_6$: Evaluation as a Cathode for Sodium Battery. *J. Power Sources* **2013**, *243*, 817–821.

(46) Sathiya, M.; Ramesha, K.; Rousse, G.; Foix, D.; Gonbeau, D.; Guruprakash, K.; Prakash, A. S.; Doublet, M. L.; Tarascon, J.-M. Li_4NiTeO_6 as a Positive Electrode for Li-Ion Batteries. *Chem. Commun.* **2013**, *49* (97), 11376–11378.

(47) Zvereva, E. A.; Nalbandyan, V. B.; Evstigneeva, M. A.; Koo, H.-J.; Whangbo, M.-H.; Ushakov, A. V.; Medvedev, B. S.; Medvedeva, L. I.; Gridina, N. A.; Yalovega, G. E.; et al. Magnetic and Electrode Properties, Structure and Phase Relations of the Layered Triangular-Lattice Tellurate Li_4NiTeO_6. *J. Solid State Chem.* **2015**, *225*, 89–96.

(48) Berthelot, R.; Schmidt, W.; Muir, S.; Eilertsen, J.; Etienne, L.; Sleight, A. W.; Subramanian, M. A. New Layered Compounds with Honeycomb Ordering: $Li_3Ni_2BiO_6$, $Li_3NiM'BiO_6$ (M′ = Mg, Cu, Zn), and the Delafossite $Ag_3Ni_2BiO_6$. *Inorg. Chem.* **2012**, *51* (9), 5377–5385.

Table of Contents Figure

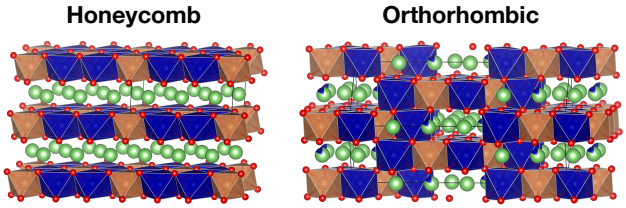

Representative crystal structures of the two distinct phases of $Li_3Co_2SbO_6$: an O3-$LiCoO_2$ type layered honeycomb structure, with a pseudo-hexagonal structure in a monoclinic *C*2/*m* unit cell; and an orthorhombic *Fddd* structure. CoO_6 octahedra are blue, SbO_6 octahedra are bronze, O atoms are red and Li atoms are green.